European Journal of Applied Physics
Vol 7 | Issue 1 | February 2025
ISSN 2684-4451

RESEARCH ARTICLE

Estimating Gravitational Redshift in Galaxy Clusters and Voids Using Hernquist and Tophat Density Profiles

Sheillah Nekesa Wekesa[1] and Dismas Simiyu Wamalwa[2,*]

ABSTRACT

Cosmic voids happen to occupy most under dense regions of the universe. They can, therefore, be used to test our theories of structure formation and cosmology. By assuming a density profile and using it to obtain the gravitational potential, the gravitational redshift is computed. The effect is compared in two profiles of clusters and voids. From the computations, the gravitational redshift in clusters is higher than that in voids, implying that if the effect is to be considered in voids, a larger survey is required. The radii used are 20 Mpc and 1 Mpc for voids and clusters respectively.

Keywords: Gravitational redshift, hernquist, tophat, voids.

Submitted: November 04, 2024

Published: February 05, 2025

10.24018/ejphysics.2025.7.1.354

[1] *Astronomy and Astrophysics Group, Department of Physics, University of Nairobi, Kenya.*
[2] *Department of Physical Sciences, Meru University of Science and Technology, Kenya.*

* ***Corresponding Author:***
e-mail: dismasw@uonbi.ac.ke

1. Introduction

Gravitational redshift is a relativistic phenomenon where light or electromagnetic radiation undergoes a wavelength increase (or frequency decrease) as it escapes a gravitational field. This shift arises from the gravitational potential difference between the emission and observation points, as predicted by general relativity. Mathematically, the gravitational redshift z is given by:

$$z = \frac{\Delta\lambda}{\lambda_0} = \frac{\lambda_{\text{obs}} - \lambda_{\text{emit}}}{\lambda_{\text{emit}}}$$

where λ_{emit} is the emission wavelength near the gravitational source, and λ_{obs} is the observed wavelength further away. Initial studies on gravitational redshift in galaxy clusters were conducted by Nottale [1], who observed redshift variations in galaxy pairs with differing richness levels, associating greater redshifts with richer clusters. Although Rood and Struble [2] repeated this test without replicating Nottale's results, Nottale [3] later identified a redshift effect where the cores of galaxy clusters appeared redshifted relative to their edges, likely due to higher gravitational potential in the core. These observations were extended by Stiavelli and Setti [4] to individual elliptical galaxies, finding a similar redshift between the cores and outer regions. Gravitational redshifts in central dominant (cD) clusters were examined by Cappi [5], who calculated velocity differences between cD galaxies and their clusters, which isolated gravitational redshift effects when averaged across clusters. Later, Broadhurst and Scannapieco [6] proposed using the redshift of metal-rich inter-cluster medium emission lines to probe gravitational redshifts by calculating emission-weighted mean potential along the line of sight.

Kim and Croft [7] advanced the field by predicting galaxy gravitational redshift within clusters through simulations based on the Cold Dark Matter (CDM) model. They found the redshift difference between the brightest cluster galaxy and other members in clusters of mass $M \sim 10^{15}\, h^{-1} M_{\odot}$ to be around ~10 km/s. Expanding on this, McDonald and Seljak [8] used Fourier space and perturbation theory to study large-scale gravitational redshift effects, while Wojtak *et al.* [9] were the first to observationally determine gravitational redshift in galaxy clusters on a large scale using the Sloan Digital Sky Survey (SDSS), revealing a net blueshift for cluster galaxies relative to the Brightest Cluster

Galaxies (BCGs). Gravitational redshift across large cosmic potentials was modeled to predict redshift variations among galaxy pairs as a function of mass and scale, linking these shifts to distortions in galaxy correlation functions [10]. Photons in a gravitational field lose energy, and their constant speed leads to wavelength increases or redshifts. Conversely, blueshift occurs when photons fall into a gravitational potential, gaining energy. This gravitational redshift z_g for static metrics can be expressed by:

$$z_g = \frac{\Delta\phi}{c^2}$$

Adopting velocity units, gravitational redshift can also be expressed as

$$\Delta v_g = \Delta z_g c = \frac{\Delta\phi}{c}$$

In addition to clusters, recent research has explored gravitational redshifts in cosmic voids, emphasizing their unique dynamical characteristics. Correa *et al*. [11] investigated voids using a spherical space finder based on statistical and theoretical methods, to identify real and redshift space voids. Void kinematics was further analyzed by Kim and Croft [7] and revealed distinct redshift patterns arising from the gravitational potentials in these underdense regions. Sheth and van De Weygaert [12] presented a hierarchical model of voids, shedding light on gravitational potential differences across void structures and suggesting void dynamics could reveal unique gravitational redshift signatures. Aragon-Calvo and Szalay [13] proposed a nested structure for voids, introducing a complex framework of subvoids with potential redshift profiles reflecting unique small-scale gravitational dynamics. Lastly, Sakuma *et al*. [14] studied gravitational redshift in void galaxies, extending analysis to gas motions within clusters and highlighting second-order Hubble effects in voids.

Collectively, these studies enhance our understanding of cosmic voids by exploring large-scale structure, gravitational potential, and redshift effects, establishing voids as significant for cosmological inquiry. In this paper, we analytically estimate gravitational redshift within galaxy clusters based on Hernquist and tophat density profiles and extend this analysis to voids using a reversed tophat model.

The paper is structured as follows: Section 1 introduces the concepts of galaxy clusters and voids. Section 2 outlines our analytical approach for estimating gravitational redshift in both clusters and voids. In Section 3, we present and discuss our findings, concluding in Section 4 with implications and future directions.

1.1. Galaxy Clusters

Galaxy clusters are the largest gravitationally-collapsed objects in the universe. They are grouped into superclusters, perhaps joined by filaments and walls of galaxies. Redshift of a galaxy is the sum of three components (Hubble redshift, Doppler redshift and gravitational redshift):

$$cz = H(z)r + v_{pec} + cz_g \tag{1}$$

where $H(z)$ is the Hubble parameter and r is the radial distance between the observer and the galaxy [7]. If galaxies are considered as sources of photons, the gravitational redshift is typically much smaller than other terms in (1). For smaller clusters, the noise from displacement of central galaxy due to Hubble expansion is significant. In most cases, the gravitational redshift component is small compared to the Hubble and Doppler terms.

For smaller clusters, however, the "noise" due to the displacement of the central galaxy becomes more pronounced. This displacement refers to the central galaxy's susceptibility to shifts caused by the weaker gravitational binding forces in smaller clusters, where peculiar velocities and Hubble flow effects introduce variability that competes with the gravitational redshift signal. Averaging redshift measurements across multiple clusters helps to reduce the impact of this noise on gravitational redshift calculations, allowing a clearer signal to emerge from these effects across large samples [9]. Cluster models inspired by data and measurements reveal [7] that transverse Doppler effect dominates over the gravitational redshift within radii $\sim 0.2\,h^{-1}$ Mpc of clusters, but at radii $r > 3\,h^{-1}$ Mpc, it drops to a very small fraction of the gravitational redshift hence, can be ignored on larger scales. The transverse Doppler effect is a relativistic phenomenon observed when the motion of an object is perpendicular to the line of sight of the observer. Unlike traditional Doppler shifts that occur due to radial (along-the-line-of-sight) motion, the transverse Doppler effect arises from the high-speed transverse (perpendicular) component of an object's motion, which causes a shift in observed frequency due to time dilation. The transverse Doppler effect is often negligible at the scales of galaxy clusters and is commonly ignored in redshift modeling, as noted by Kim and Croft [7], where peculiar velocities and gravitational influences dominate the redshift measurement. Potential wells are deeper for most

massive clusters which result into larger gravitational redshifts and consequently, give rise to a net blue-shift of the other cluster members relative to the Brightest Cluster Galaxy (BCG). The brightest galaxy is selected from each cluster. BCG lying within 0.1 Mpc of the cluster center is defined as a "central BCG".

In virialised clusters, the transverse Doppler effect is generically present alongside gravitational redshift because of virial theorem which relates potential and kinetic energies of galaxies.

There are other factors to be considered while making an interpretation of the measurement of off-set blueshift of other cluster galaxies relative to the central BCG apart from the transverse Doppler effect. Key elements include peculiar velocities of galaxies within clusters, systematic observational biases, and local environmental influences, which can collectively introduce additional redshift or blueshift signals These factors can easily be estimated from the already measured line-of-sight velocities and subtracted from blue-shift to obtain the net blue-shift.

1.2. Voids

Voids are large, relatively empty regions of space that contain significantly fewer galaxies and matter than the surrounding areas. They have sizes of about $20 - 50\,h^{-1}$ Mpc that are practically without or with very few galaxies. They occupy the most underdense regions in the universe, and constitute the dominant fraction of it. They are promising independent probes to test our theories of structure formation and cosmology [15], [16].

Although voids are devoid of matter by definition, one can still find galaxies in their interior. Physics of galaxies in voids is simpler since, the non-linear effects of gravity are less significant in regions of space devoid of galaxies.

2dF Galaxy Redshift Survey (2dFGRS) and Sloan Digital Sky Survey (SDSS) provided the largest samples of voids and galaxies which could be used to measure their properties statistically. Hoyle and Vogeley [17] applied void finder algorithm to the 2dFGRS dataset and found voids to have a typical radius of $15h^{-1}$ Mpc.

Many small voids may coexist within one larger void leading to Hierarchical evolution of voids. However, in our model, we take the overal view that voids evolve as isolated objects.

2. Analytical Estimates of Gravitational Redshift

The gravitational redshift in any given mass is obtained by suppossing a density profile and using it to compute the gravitational potential as a function of redshift. The difference between the value at the centre and the oustskirts of a cluster gives us the expected effect. The observed luminosity density profile of regular clusters is reasonably fitted by de Vaucouleurs law [3], [5]:

$$\sigma(R) = \sigma_e exp\left[-7.67\left(\left(\frac{R}{R_e}\right)^{\frac{1}{4}} - 1\right)\right] \tag{2}$$

where $\sigma(R)$ is the surface density at projected distance, R, from the center and σ_e is the surface density at the effective radius, R_e. Unfortunately, this law has so far led to non-analytical de-projection quantities. Hernquist proposed a density distribution which is a prototype of de-projected version of the de Vaucouleurs law from which the spatial gravitational redshift profile could be obtained.

2.1. Hernquist Profile

Hernquist profile is used to describe density of spherically elliptical galaxies. The choice of the Hernquist profile in our study is driven by its mathematical simplicity, physical interpretability, and suitability for our specific analytical objectives. This profile, in terms of density distributions, is a special case of the profile:

$$\rho(r) = \frac{\rho_0}{\left(\frac{r}{a}\right)^{\alpha}\left(1 + \frac{r}{a}\right)^{\beta-\alpha}} \tag{3}$$

For $\alpha = 1,\ \beta = 4$, we have

$$\rho(r) = \frac{Ma}{2\pi r(r+a)^3} \tag{4}$$

where a is the characteristic length scale of the system approximated in terms of the effective radius R_e as $R_e/1.8153$ and M is the total mass of the system. But the amount of mass in the spherical system bounded by the sphere of radius r (cumulative mass distribution, $M(r)$) is given by:

$$M(r) = \int_0^{2\pi}\int_{-\pi/2}^{\pi/2}\int_0^r \rho(r) r^2 sin\theta\, dr d\theta d\phi = 4\pi \int_0^r \rho(r) r^2 dr \tag{5}$$

Using (4) in (5) gives:

$$M(r) = 4\pi \int_0^r \frac{M}{2\pi}\frac{a}{r}\frac{1}{(r+a)^3}r^2 dr = 2Ma\int_0^r \frac{r}{(r+a)^3}dr \tag{6}$$

Integration by parts reduces (6) to:

$$M(r) = \left[\frac{-ar}{(r+a)^2}\right]_0^r - \left[\frac{-a}{(r+a)}\right]_0^r \tag{7}$$

This leaves us with a slight problem at $r = 0$, which can be resolved as:

$$\int_0^r = \int_0^\infty - \int_r^\infty \tag{8}$$

But total mass

$$M = \int_V \rho(r)dV = 4\pi \int \rho(r)r^2 dr \tag{9}$$

so that $M(r)$ can be written in terms of total mass M in the form:

$$M(r) = M\frac{r^2}{(r+a)^2} \tag{10}$$

Using (10), we can obtain the potential $\phi(r)$ of the system by integrating the poisson equation:

$$\phi(r) = -G\int_r^\infty \frac{M(r)}{r^2}dr = -GM\int_r^\infty \frac{dr}{(r+a)^2} \tag{11}$$

The potential for the Hernquist profile can easily be reduced to the form:

$$\phi(r) = -\frac{GM}{(r+a)} \tag{12}$$

Spatial gravitational redshift profile is thus given by:

$$V_H = -\frac{\phi(r)}{c} = \frac{GM}{c(r+a)} \tag{13}$$

2.1.1. *Gravitional Redshift Using Hernquist Model*

To obtain the gravitational redshift of the cluster, v_c, the mass-weighted spatial gravitational redshift profile, V_H, is integrated over radius, r_c, of the cluster as:

$$v_c = \frac{\int_0^{r_c}\rho(r)V_H(r)dV}{\int_0^{r_c}\rho(r)dV} = \frac{GM}{c}\frac{\int_0^{r_c} r/(a+r)^4 dr}{\int_0^{r_c} r/(a+r)^3 dr} \tag{14}$$

This integral can be performed and simplified by matlab to give the following result:

$$v_c = \frac{-GM(a+3r_c)}{6c(a+r_c)^3\left(\frac{a}{2(a+r_c)^2} - \frac{1}{a+r_c}\right)} \tag{15}$$

For virialised clusters, we re-write the total mass in terms of $M(<a)$ so that (15) becomes:

$$v_c = \frac{-4GM(<a)(a+3r_c)}{6c(a+r_c)^3\left(\frac{a}{2(a+r_c)^2} - \frac{1}{a+r_c}\right)} \tag{16}$$

where the factor 4 is obtained from (10) as $r \to a$, i.e., $M = 4M(<a)$. But

$$M(<a) = \frac{4\pi a^3}{3}200\rho_{crit} = \frac{100H2a^3}{G} \tag{17}$$

where the critical density ρ_{crit} is defined in terms of Hubble parameter H and cluster radius a to be described later. Equation (16) can now be rewritten as:

$$v_c = \frac{-400H^2a^3(a+3r_c)}{6c(a+r_c)^3\left(\frac{a}{2(a+r_c)^2} - \frac{1}{a+r_c}\right)} \tag{18}$$

This equation represents the gravitational redshift of a photon moving from the centre of a virialised galaxy cluster to its edges.

2.2. Tophat Model

In this model, the tophat density profile is defined as [3], [5], [16]:

$$\rho(r) = \begin{cases} constant, & r < a \\ 0, & r > a \end{cases} \tag{19}$$

This model assumes that the formation of bound objects in the universe can in the first approximation be described by evolution of a uniformly overdense region. The physical significance of using a tophat density profile lies in its ability to model large, relatively uniform regions effectively, setting clear boundaries and simplifying gravitational potential estimations. This allows for straightforward gravitational redshift estimations in contexts such as galaxy clusters and cosmic voids, making it an insightful tool for exploring gravitational interactions in a cosmological context. To obtain the constant, we consider how our density perturbation evolves to a maximum size $r = r_{max}$ at time $t = t_{max}$ and then collapse within a finite time. We take the shells of this model within the density perturbation to have similar self trajectories (the mass within each shell is the same) so that turnaround occurs at the same time. Turnaround occurs when the object is at its maximum size so that it has no kinetic energy at that instant giving the total energy E as:

$$E = \frac{-GM}{r_{max}} \tag{20}$$

The particles in different shells cross each other and the object virialises so that:

$$W_{vir} = -2K_{vir} \tag{21}$$

where W_{vir} is the potential energy while K_{vir} is the kinetic energy. We assume conservation of energy of the system from the time of turnaround to the time it virialises, so that

$$E = W_{vir} + K_{vir} = \frac{1}{2} W_{vir} \tag{22}$$

and hence,

$$\frac{GM}{2r_{vir}} = \frac{GM}{r_{max}} \tag{23}$$

Virial radius is the radius around a cluster within which the density is $200\rho_{crit}$. From (23), the ratio of halo's virial radius to turnaround radius is 2. This value cubed gives the collapsing sphere's fractional change in volume which implies that the density within our volume has increased by a factor of 2^3 while that of background density has increased by a factor of 2^2 since $\rho \propto a^{-3}$ and $a \propto t^{2/3}$ in a matter-dominated universe. The actual non-linear density contrast at turnaround is $6\pi^2/4^3$. After virialisation, the overdensity within our volume will have grown from 5.5 to $5.55 \times 8 \times 4 \approx 178$. Usually, this value is approximated to 200 and is taken to describe overdensity of a collapsed object. Thus;

$$\rho(r) = 200\rho_{crit} \tag{24}$$

where ρ_{crit} is derived from Friedmann's equation:

$$\left(\frac{dlna}{dt}\right)^2 + \left(\frac{kc^2}{R_0 a(t^2)}\right) = \frac{8\pi G\rho}{3} \tag{25}$$

For a flat universe ($\kappa = 0$),

$$\rho_{crit} = \frac{3H^2}{8\pi G} \tag{26}$$

This profile can be understood by considering a cluster whose background was initially expanding but eventually pulled away from the background expansion and collapsed after reaching its maximum size. This happens if the object is denser than its background.

2.2.1. Gravitational Redshift Using Tophat Model

If we again assume our cluster to be a uniform sphere, the mass within the radius of cluster as given by (5) is:

$$M(< r) = 4\pi \int_0^r \rho(r) r^2 dr = \frac{800\pi\rho_{crit} a^3}{3} \tag{27}$$

so that total mass for the cluster of radius a is

$$M = \frac{800\pi\rho_{crit}a^3}{3} \tag{28}$$

From (11), the potential for a cluster of radius a becomes:

$$\phi(r) = -G\int_r^a \frac{M(r)}{r^2}dr = -100H^2\int_r^a rdr = -50H^2(a^2 - r^2) \tag{29}$$

The spatial gravitational redshift (V_T) for the tophat model is given by: b

$$V_T = \begin{cases} \dfrac{50H^2(a^2 - r^2)}{c}, & r < a \\ 0, & r > a \end{cases} \tag{30}$$

Similar to the Hernquist model, the gravitational redshift of the cluster (v_c) for the tophat model can be calculated by integrating over the mass weighted V_T as:

$$v_c = \frac{\int_0^{r_c} \rho V_T(r)dV}{\int_0^{r_c} \rho dV} \tag{31}$$

to give

$$v_c = \frac{50H^2a^2}{c}\left(1 - 0.6\frac{{r_c}^2}{a^2}\right) \tag{32}$$

where we have combined (26), (28), (30) and (31).

2.3. Gravitational Redshift in Voids Using Reverse Tophat Model

Voids are under dense structures that to a first approximation have simple structure and dynamics. They are spherical objects devoid of galaxies thus, are extremely empty in the center and show an increase in density towards their edges. This implies that their gravitational force decreases towards the center leading to expansion. As a consequence, the matter within voids move from interior and accumulate to the boundaries. This leads to a void density which evolve towards a reversed tophat (with a uniform interior density depression and a steep outer boundary) profile given as:

$$\rho = \begin{cases} 0.2\rho_{crit}, & r < a \\ 2\rho_{crit}, & a < r < b \\ 0, & r > b \end{cases} \tag{33}$$

where $0.2\rho_{crit}$ is the density of the void and $2\rho_{crit}$ is the density of the wall. The choice of wall density as $2\rho_{crit}$ in the reverse tophat profile for voids is motivated by the spherical expansion model, supported by empirical findings and simulations that show consistent density contrasts in void walls [12] and observational support from large-scale galaxy surveys. To find the thickness of the wall, we take the missing mass in the void to be the one that forms the wall. For constants f and A, let the density of the void and the wall be $f\rho_{crit}$ and $A\rho_{crit}$ respectively. This implies that we can equate their masses

$$\frac{4\pi a^3(1-f)\rho_{crit}}{3} = 4\pi\rho_{crit}\int_a^b (A-1)r^2dr \tag{34}$$

As outlined above, $f = 0.2$ and $A = 2$ so that substituting these values in (34), we obtain $b/a = 1.2$. We further need the potential of both the void and the wall considering the fact that the two have different signs. Unlike for the cluster, the gravitational potential of the void increases from the center. Since we are assuming a spherical shape, the contribution of the potential outside the sphere is zero. a and $b-a$ are the radii of the sphere for the void and the wall respectively. The gravitational potential is the sum of the two contributions. See (11) for the gravitational potential due to the void and the wall:

$$\phi(r) = G\int_r^a \frac{M(<r')}{r'^2}dr - G\int_a^{1.2a} \frac{M(<r')}{r'^2}dr \tag{35}$$

The gravitational potential of the void is obtained as:

$$M(<r') = 4\pi(0.2\rho_{crit})\int_0^r r'^2dr = \frac{0.1H^2r^3}{G} \tag{36}$$

Similarly, the gravitational potential of the wall can be shown to be:

$$M(<r') = 4\pi(2\rho_{crit})\int_0^r r'^2 dr = \frac{H^2 r^3}{G} \tag{37}$$

Using (36) and (37) in (35), we obtain:

$$\phi(r) = \frac{0.1H^2(a^2 - r^2) - H^2(1.44a^2 - a^2)}{2} \tag{38}$$

The spatial gravitational redshift is thus given by:

$$V_v = H^2 \frac{0.03r^2 + 0.17a^2}{c} \tag{39}$$

where $a = 20\ Mpc$. This gives the gravitational redshift of the void as:

$$v_v = \frac{\int_0^{r_c} \rho V_T(r) dv}{\int_0^{r_c} \rho dv} \tag{40}$$

Substituting (33) and (39) into (40), we obtain:

$$v_v = \frac{H^2(0.03r^2 - 0.34a^2)}{c} \tag{41}$$

3. Results and Discussion

3.1. Hernquist Model

To see how gravitational redshift varies with radius in a cluster, the result of (18) is plotted as shown in Fig. 1. As expected, the central galaxy has the highest gravitational redshift which, from the plot is ~2.30 km/s while at the edge of the cluster is ~1.52 km/s. This is because photons coming from the deepest point of the potential well lose more energy as compared to other points. This can be attributed to variation in gravitational potential which depends on the distribution of mass in the cluster. The galaxy at the center is the most massive so lies in the deepest potential wells producing larger effect of gravitational redshift. We have considered the mass of the cluster to be given by $10^{14}\, h^{-1} M_\odot$ while a is the cluster radius given as $0.713\, h^{-1}\ Mpc$. If we consider in the limit when the radius r tends to radius of the cluster, from the plot, we find a difference of ~0.78 km/s. In our plot, we have only considered one cluster and determined how gravitational redshift changes from its centre.

We can then compute the difference between the central galaxy and the galaxy at the edges of the cluster. In our calculations, we consider virialised cluster. The gravitational redshift of the central galaxy is estimated by integrating (14) from a to $0.1\, a$ to get ~6.95 km/s where we have taken the value

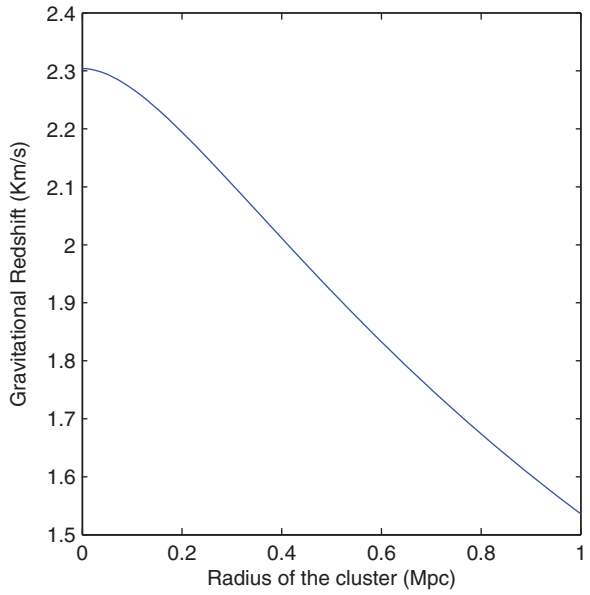

Fig. 1. Gravitational redshift in a cluster using Hernquist profile plot.

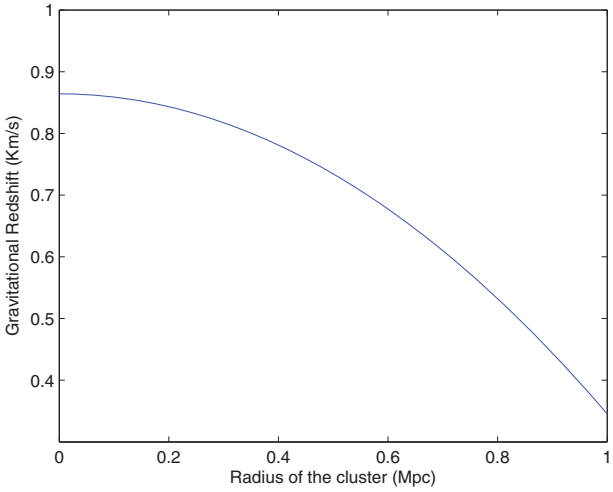

Fig. 2. Tophat gravitational redshift plot.

of a to be 1 Mpc. The effect can also be approximated for a galaxy towards the edge of the cluster by integrating this time from $0.9a$ to a to obtain ∼3.55 km/s. To observe the effect, the difference between the value at the edges of the cluster is usually subtracted from the value at the center. In our case, we obtain a difference of $3.40\,km/s$ from which, we can deduce that there is a blueshift of the galaxies at the edge of the cluster relative to the central galaxy as expected. As mentioned earlier, Kim and Croft [7] using simulated clusters found the difference in gravitational redshift between the central galaxy and the other galaxies to be $\sim 10\,km/s$ for clusters of mass $10^{15}\,h^{-1}M_{\odot}$.

3.2. Tophat Model

To see how the gravitational redshift of the virialised object of this model varies with the radius of the cluster, we make a plot of (32) as shown in Fig. 2. From the graph, we see that the gravitational redshift gets smaller as we move away from the centre of the virialised cluster but not as rapidly as that of hernquist model. The gravitational redshift between the central galaxy and the galaxy at the edge of the cluster is ∼0.66 km/s from the plot. In the same way we computed gravitational redshift of the central galaxy for the hernquist, we can also find the value for tophat profile by integrating (31) from 0 to 0.1a to get ∼0.86 km/s. To obtain the effect at the edge of the cluster, we integrate from 0.9 a to a to yield ∼0.08 km/s. The difference is thus ∼0.78 km/s. There is again a blueshift of the galaxies at the edge of the cluster relative to the central galaxy.

3.3. Voids (Reversed Tophat Model)

Gravitational redshift of the void as it varies with radius from the centre is plotted from (41) and shown in Fig. 3. From the graph, the difference between gravitational redshift at the centre and at the edge of the void is ∼−0.2 km/s. Integrating (40) from 0 to 0.1a, and noting that $a = 20\,Mpc$ for the void, we obtain the gravitational redshift at the centre of the void to be ∼1.18 km/s. We next consider the gravitational redshift at the edge of the void (wall) by integrating from 0.9 a to a to get ∼1.49 km/s. The difference between the gravitational redshift at the centre of the void and that at the edge of the void is therefore ∼−0.31 km/s. Unlike for a cluster, a void has a blue shift at the centre and thus, the gravitational redshift increases away from it. Photons travel from weaker fields to stronger fields hence,

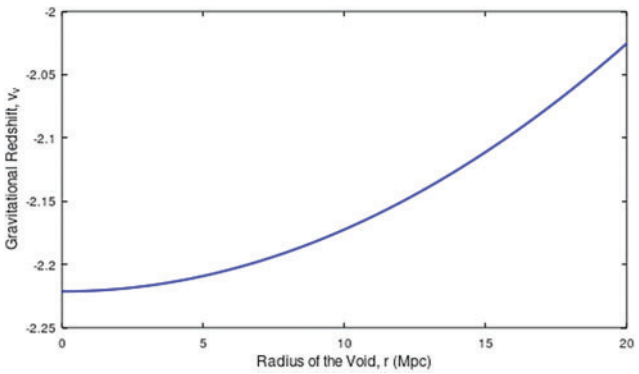

Fig. 3. Gravitational redshift of the void as it varies with radius from the centre.

get blueshifted. There is a redshift from the edges of the void relative to its centre. We expect a redshift as the photons pass through the wall but the effect of blues-shift is greater giving the net effect as a blue shift.

4. Summary and Conclusions

In this paper, gravitational redshift is estimated in clusters and voids analytically by assuming a density profile. This effect depends on the distribution of mass in the cluster. More massive galaxies lie in deeper potential wells hence, the photons lose a lot of energy as they climb out of them. From our calculations, the galaxies surrounding the central galaxy have a relative blueshift as predicted by GR. Hernquist profile whose mass is highly distributed at the centre gives a higher effect than the tophat model. Furthermore, for these two models, the galaxies at the edges of the cluster are blueshifted relative to the central galaxy. The errors in the measurement of gravitational redshift can be averaged out by summing many galaxies in different clusters. Although both profiles are modeled for clusters, the effect is larger for hernquist than for tophat. This can be explained from the fact that the density profiles is steeper for hernquist at the centre than tophat. Gravitational redshift for the hernquist profile reduces rapidly from the centre of the cluster hence, gives higher differences of the effect between the central galaxy and the other cluster members. While the gravitational redshift is indeed proportional to the difference in gravitational potential at the center and at the edge of a dark matter halo, the slope of the density profile does influence the distribution of mass within the halo and, consequently, the potential profile. Although two halos may exhibit the same gravitational potential difference, a steeper density profile, such as that of the Hernquist model, implies a more concentrated mass distribution towards the center compared to the tophat model, which has a more uniform density profile. This variation in mass distribution can affect the dynamics of galaxies within the halo, their velocities, and the resulting redshift measurements. Thus, while the gravitational potential difference may remain the same, the underlying density profile can lead to different physical implications and interpretations in the context of gravitational redshift. Since voids occupy a large volume of the universe, they should also be used to test the theories of structure formation in Physics. Measuring gravitational redshift in voids provides valuable insights into the dynamics of cosmic structure formation due to several factors. First, voids represent underdense regions of the universe where the gravitational influence of surrounding structures is diminished. By analyzing the gravitational redshift of galaxies situated at the edges of voids, we can gain information about the gravitational potential in these low-density environments, helping to refine our models of dark matter distribution and its role in structure formation.

Second, the study of gravitational redshift in voids allows researchers to investigate the effects of large-scale cosmic flows and the motion of galaxies within these regions. Understanding how galaxies move and interact in voids can illuminate the processes of collapse and growth that lead to the formation of large-scale structures, such as filaments and clusters.

Moreover, gravitational redshift measurements in voids can provide constraints on the evolution of the universe, particularly regarding dark energy and its influence on the expansion rate. As voids are crucial for testing the homogeneity and isotropy of the universe, these measurements can help us assess the validity of cosmological models and improve our understanding of the interplay between dark matter, dark energy, and cosmic structure formation. The density profile of the void is such that it increases away from its centre. We thus modelled it by considering reverse tophat model. The centre of the void has a greater blueshift than the edges. This is because its mass increases outwards. The effect is larger in clusters than in voids. This effect can be seen if we compare $GM_c/a_c c^2$ with $GM_v/a_v c^2$ to get $200\rho_{crit}a_c^2/0.2\rho_{crit}a_v^2$ where subscripts c and v denote cluster and void respectively. Thus, the ratio of the effect of the cluster to void is $\sim$2.5 where, as before, we have used the radius of the void and radius of the cluster to be 20 Mpc and 1 Mpc respectively. We thus, see that the effect is larger in clusters. For virialised clusters, $E = W/2 = GM/R$. All virialised clusters have $M/R^3 \sim$ constant. Hence, $E \sim M^{2/3}$. From the chameleon mechanism for high energy density, GR is retrieved on small scales. From $E \sim M^{2/3}$, smaller clusters have smaller energies. For this reason, virialised clusters might not be very good tests. Virialized clusters, while they are indeed massive and could, in principle, produce a more substantial signal for the chameleon mechanism, may not be the ideal candidates for several reasons. First, the virialization process indicates that these clusters have reached a dynamic equilibrium, where the gravitational binding energy is balanced by the thermal energy of the galaxies within the cluster. This equilibrium state can mask the effects of modified gravity theories, such as those predicted by the chameleon mechanism, which may be more prominent in regions with lower gravitational binding and density contrasts.

Furthermore, the presence of a dense concentration of galaxies and dark matter in virialized clusters leads to a complex interplay of gravitational forces that can obscure modifications to gravity that the chameleon mechanism proposes. High-mass clusters might indeed exhibit a larger signal, but this signal

may be difficult to isolate due to competing effects, such as baryonic physics, non-linear structures, and the potential dilution of the chameleon effect in the strong gravitational fields of these clusters.

In contrast, voids offer a unique environment where the influence of gravity is weaker, allowing for clearer observations of the chameleon mechanism's effects without the confounding factors present in dense cluster environments. The low density and relative isolation of voids may make them more sensitive to the alterations in gravitational behavior predicted by the chameleon mechanism, thus providing a more straightforward test of such theories.

Therefore, while high-mass clusters are certainly of interest, exploring gravitational redshift in voids remains a valuable approach for testing the chameleon mechanism and understanding its implications for structure formation and cosmic evolution. However, if this is to be done, a larger survey is required. This will constitute our next task.

Acknowledgment

The authors would like to thank Intenational Centre for Theoretical Physics (ICTP) for its financial support of this research in terms of travel and stay at ICTP to one of the authors. We would also like to thank the University of Nairobi for providing us with resourc e materials and conducive work environment while writing this paper. We further ackwnoledge useful discussions with Prof. Sheth Ravi of Intenational Centre for Theoretical Physics (ICTP) regarding this research.

Conflict of Interest

The authors declare that they do not have any conflict of interest.

References

[1] Nottale L. Redshift anomaly in associations of clusters of galaxies? *Astrophys J Lett*. 1976;208:L103. doi: 10.1086/182242.
[2] Rood HJ, Struble MF. Test for a richness-dependent component in the systemic redshifts of galaxy clusters. *Astrophys J, Part 2-Lett Ed*. 1982 Jan 1;252:L7–10.
[3] Nottale L. Gravitational lensing as a probe for dark matier. In *And cosmic structures*. 1990, pp. 171.
[4] Stiavelli M, Setti G. Non-equilibrium motions in galaxies and gravitational redshift. *Mon Not R Astron Soc*. 1993;262(1):L51–4. doi: 10.1093/mnras/262.1.L51.
[5] Cappi A. Gravitational redshift in galaxy clusters. *Astron Astrophys*. 1995;301:6.
[6] Broadhurst T, Scannapieco E. Detecting the gravitational redshift of cluster gas. *Astrophys J*. 2000;533(2):L93. doi: 10.1086/312630.
[7] Kim YR, Croft RA. Gravitational redshifts in simulated galaxy clusters. *Astrophys J*. 2004;607(1):164. doi: 10.1086/383218.
[8] McDonald P, Seljak U. How to evade the sample variance limit on measurements of redshift-space distortions. *J Cosmol Astropart Phys*. 2009;2009(10):007. doi: 10.1088/1475-7516/2009/10/007.
[9] Wojtak R, Hansen SH, Hjorth J. Gravitational redshift of galaxies in clusters as predicted by general relativity. *Nature*. 2011;477(7366):567–9. doi: 10.1038/nature10445.
[10] Croft RA. Gravitational redshifts from large-scale structure. *Mon Not R Astron Soc*. 2013;434(4):3008–17. doi: 10.1093/mnras/stt1223.
[11] Correa CM, Paz DJ, Sánchez AG, Ruiz AN, Padilla ND, Angulo RE. Redshift-space effects in voids and their impact on cosmological tests. Part I: the void size function. *Mon Not R Astron Soc*. 2021;500(1):911–25. doi: 10.1093/mnras/staa3252.
[12] Sheth RK, Van De Weygaert R. A hierarchy of voids: much ado about nothing. *Mon Not R Astron Soc*. 2004;350(2):517–38. doi: 10.1111/j.1365-2966.2004.07661.x.
[13] Aragon-Calvo M, Szalay A. The hierarchical structure and dynamics of voids. *Mon Not R Astron Soc*. 2013;428(4):3409–24. doi: 10.1093/mnras/sts281.
[14] Sakuma D, Terukina A, Yamamoto K, Hikage C. Gravitational redshifts of clusters and voids. *Phys Rev D*. 2018;97(6):063512. doi: 10.1103/PhysRevD.97.063512.
[15] Van de Weygaert R, Platen E. Cosmic voids: structure, dynamics and galaxies. *International Journal of Modern Physics: Conference Series*, vol. 1, pp. 41–66, World Scientific, 2011.
[16] Hamaus N, Sutter P, Wandelt BD. Universal density profile for cosmic voids. *Phys Rev Lett*. 2014;112(25):251302. doi: 10.1103/PhysRevLett.112.251302.
[17] Hoyle F, Vogeley MS. Voids in the two-degree field galaxy redshift survey. *Astrophys J*. 2004;607(2):751. doi: 10.1086/386279.